DOI: 10.2478/cdem-2025-0006 CHEM DIDACT ECOL METROL. 2025;30(1-2):47-65

Mohammad GHEIBI[1,2*], Zahra HAJIAHMADI[1], Katarzyna JAROMIN-GLEŃ[3]
Mohammad EFTEKHARI[4], Kourosh BEHZADIAN[5,6], Miroslav ČERNÍK[1]
and Stanisław WACŁAWEK[1]

AI-BASED EXPERT SYSTEM DESIGN FOR OPTIMISATION OF HEAVY METAL ADSORPTION ON WASTE-DERIVED ADSORBENTS

Abstract: Heavy metal contamination in wastewater is a major global problem that requires effective, automated, and sustainable treatment systems capable of linking laboratory-scale adsorption processes to intelligent large-scale operation. This work introduces a novel Expert System (*ES*) that combines a Genetic Algorithm (*GA*), Artificial Neural Networks (*ANN*), and Monte Carlo (*MC*) analysis for the automated removal of heavy metals using adsorbents obtained from Low-Density Concrete waste. This research is significant because adsorption systems are complex to automate due to their nonlinear behaviour and sensitivity to fluctuating operating conditions. By facilitating intelligent process control and optimisation, the system overcomes the main drawback of adsorption technology, which is its lack of automation. Experimental datasets for Pb^{2+}, Co^{2+} and Mn^{2+} removal were used to train the *ANN*, which predicts removal from inputs (pH, adsorbent mass, contact time, initial concentration). *GA* then used this trained *ANN* to optimise these same factors. According to the sensitivity analysis, the most important control variables in heavy metal adsorption were heavy metal type, pH, and adsorbent mass. The ANN model demonstrated strong predictive performance (R^2 = 0.908, RMSE = 7.43 %), enabling GA to optimise process conditions and achieve removal efficiencies of 100 % (Pb^{2+}), 87.8 % (Co^{2+}), and 71.62 % (Mn^{2+}) under identified optimal operating parameters. Operational reliability measured by *MC* simulations showed Co^{2+} had a higher variability (*CV*: Coefficient of Variation = 5.39 %) than Mn^{2+} (*CV* = 3.29 %) and Pb^{2+} (*CV* = 2.13 %), which had minimal uncertainty. Using resources from the circular economy, the *ES* provides a framework for a digital twin of an Industry 4.0-compliant water treatment system that enables translation of lab-based procedures into practical applications.

Keywords: expert system, heavy metal adsorption, machine learning, construction and demolition waste, water treatment plant, process automation, Industry 4.0

[1] Institute for Nanomaterials, Advanced Technologies and Innovation, Technical University of Liberec, Bendlova 6, 460 01 Liberec, Czech Republic, ORCID: MG 0000-0003-1987-5790, ZH 0009-0003-5230-4858, MČ 0000-0002-7554-020X, SW 0000-0002-8430-8269
[2] Faculty of Mechatronics, Informatics, and Interdisciplinary Studies, Technical University of Liberec, Hálkova 917, 461 17 Liberec-Staré Město, Czech Republic
[3] Institute of Agrophysics, Polish Academy of Sciences, ul. Doświadczalna 4, 20-290 Lublin, Poland, ORCID: 0000-0002-6015-3477
[4] Department of Chemistry, Faculty of Sciences, University of Neyshabur, Iran, ORCID: 0009-0008-0062-029X
[5] Centre for Urban Sustainability and Resilience, Department of Civil, Environmental and Geomatic Engineering, University College London, Gower St, Bloomsbury, London, WC1E 6BT, United Kingdom, ORCID: 0000-0002-1459-8408
[6] School of Computing and Engineering, University of West London, St Mary's Rd, London, W5 5RF, United Kingdom
[*] Corresponding author: mohammad.gheibi@tul.cz

Abbreviations	Descriptions
ANFIS	Adaptive Neuro-Fuzzy Inference System
ANN	Artificial Neural Networks
AVG	Average
BP	Back Propagation
CDF	Cumulative Distribution Function
CI	Confidence Intervals
CNN	Convolutional Neural Network
CT	Contact Time
CV	Coefficient of Variation
DSS	Decision Support System
ES	Expert System
GA	Genetic Algorithm
IC	Initial Concentration
IoT	Internet of Things
KPI	Key Performance Indicators
LDC	Low-Density Concrete
MA	Mass of Adsorbent
MAD	Median Absolute Deviation
MAE	Mean Absolute Error
MC	Monte Carlo
MI	Mutual Information
ML	Machine Learning
MSE	Mean Squared Error
NMI	Normalised Mutual Information
PCA	Principal Component Analysis
PDF	Probability Density Function
R^2	Coefficient of Determination
RF	Random Forest
RMSE	Root Mean Square Error
RP	Removal Percentage
RSM	Response Surface Methodology
SD	Standard Deviation
SHAP	Shapley Additive Explanations
SVM	Support Vector Machines
UN SDGs	United Nations Sustainable Development Goals

Introduction

With continuous technological progress and societal development, rapid industrialisation and urban expansion have led to an increase in the release of hazardous substances, particularly heavy metals [1, 2]. The presence of these contaminants adversely affects the quality of soil and water, disrupts associated ecosystems, and poses significant risks to human health [3]. Compared with membrane, chemical, electrochemical, biological [4, 5] and photocatalytic methods, adsorption [6] remains the most cost-effective, well-established, and environmentally friendly technique for heavy metal [7-9] removal in wastewater treatment. Adsorption provides operational simplicity and high removal

efficiency even at low metal concentrations. In contrast, membrane and electrochemical systems, though offering greater automation, are generally more complex and costlier. The main limitation of adsorption techniques is their limited ability to be automated, which restricts their continuous and large-scale application. However, adsorption continues to be a practical and extensively used method for the long-term removal of heavy metals [10]. Machine Learning (*ML*) plays a crucial role in automating adsorption processes for heavy metal removal by enabling accurate prediction, optimisation, and control of operational parameters [11]. Reducing experimental effort, algorithms such as Artificial Neural Network (*ANN*) [12], Support Vector Machines (*SVM*) [13], and Random Forest (*RF*) [14] can simulate nonlinear interactions between variables, e.g., pH, adsorbent dose, and contact time. The integration of *ML* with sensors and control systems enhances real-time monitoring, facilitates adaptive decision-making, and automates adsorption-based wastewater treatment effectively.

The automation, design, and predictive modelling of adsorption processes for the removal of heavy metals have been greatly enhanced by recent developments in *ML*. In order to discover important factors that have an impact on adsorption, such as synthesis and ambient conditions, Liang et al. [15] applied *ML* to Schwertmannite, a sea urchin-like adsorbent, using an *RF* model trained on 814 data groups with 27 attributes. Leng et al. [16] optimised pyrolysis settings using only biomass composition data by using a hybrid *ML* framework that combines relationships between biomass, production, biochar, and application to predict biochar characteristics and adsorption behaviour. In order to improve soil remediation techniques, Wang et al. [17] used a variety of *ML* models, most notably XGBoost, to pinpoint important soil characteristics that affect heavy metal adsorption, such as pH, reactive oxides, and organic matter. In a similar vein, Yaseen and Alhalimi [18] combined ensemble *ML* techniques including XGBoost, LightGBM, and Adaboost to forecast the adsorption efficiency of biochar-based heavy metal, emphasising the crucial roles of pH and metal-to-biochar ratios.

The adsorption capacity of geopolymers was predicted by Han et al. [19] using an Extra Trees model, which ranked feature importance based on parameters including pH, dose, and curing time. In order to simulate biochar sorption efficiency, Hassan et al. [20] used a combination of linear, nonlinear, and deep learning methods, such as *ANN*, Convolutional Neural Network (*CNN*), and CatBoost. They also used Shapley Additive Explanations (*SHAP*) analysis for automated performance evaluation and feature interpretation. Tank et al. [21] created amine-modified mesoporous silica, applied 14 *ML* algorithms using *SHAP*-based feature dependency analysis, and created a stacking regressor to improve adsorption performance prediction.

To forecast the ion exchange resin adsorption capacity for heavy metals, Xu et al. [22] created a library of resin adsorption data by combining LightGBM modelling with attributes gained from molecular simulations. Wang et al. [23] used regression, *ML*, and deep learning models to study heavy metal adsorption onto microplastics. *RF* produced the best prediction and identified environmental factors as the main adsorption determinants. Overall, these studies show how *ML* may revolutionise adsorbent synthesis, feature selection, and system automation, enabling the development of intelligent and flexible adsorption-based decontamination systems.

The intricacy of waste-derived materials, whose heterogeneous and mixed surfaces make adsorption modelling and automation difficult [24], has not been addressed in previous studies that have applied *ML* to a variety of adsorbents. By combining

metaheuristic algorithms with *ML* models, an Expert System (*ES*) framework is created in this study to bridge this gap. This results in a novel Decision Support System (*DSS*) that allows for automated control, prediction, and intelligent optimisation of heavy metal adsorption using waste-based adsorbents.

According to the identified research gap, the present study aims to develop a comprehensive dataset from experimental adsorption processes of heavy metals using Low-Density Concrete (*LDC*) [25] as the adsorbent. An *ML* model based on the *ANN* is then constructed to predict the Adsorption Performance. Subsequently, GA optimisation is performed using the trained ANN to identify optimal operating conditions. The model's uncertainty is evaluated through Monte Carlo (*MC*) analysis, and finally, its performance is validated under a simulated water treatment plant with synthetic data in the range of experimental conditions to assess the overall efficiency of the developed *ES*.

Materials and methods

The research program starts with gathering experimental data on heavy metal adsorption utilising adsorbents produced from construction and demolition waste (LDC), as shown in Figure 1. Significant parameters are then found by statistical analysis. Adsorption performance is predicted by the *ML* stage (*ANN*), and then important variables are optimised by using the meta-heuristic *GA*. Model uncertainty is then assessed using *MC* analysis. Lastly, all phases are integrated for automated adsorption process prediction, optimisation, and control using the built *ES*.

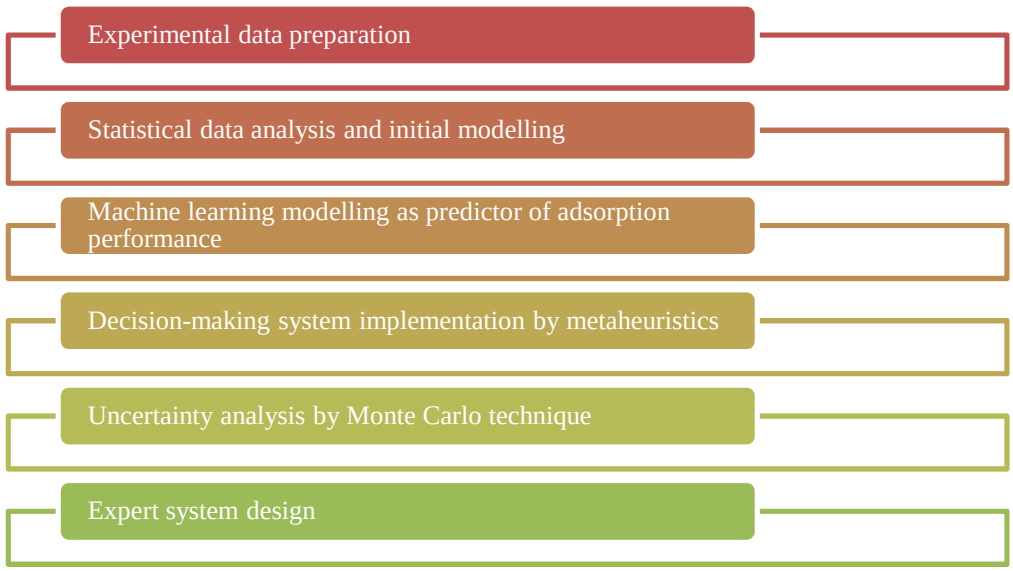

Fig. 1. The research roadmap of the present study

Experimental steps and dataset preparation

This study prepares the dataset based on the study of Gheibi et al. [25]. Experimental data on the adsorption of Pb^{2+}, Co^{2+}, and Mn^{2+} ions [26] (designated as 1-3) onto *LDC* adsorbent are included in the dataset. All experiments were conducted in single-contaminant reactors. Parameters including (1) pH (2-5), (2) Mass of Adsorbent (*MA*) (1.33-10) g/L, (3) Contact Time (*CT*) (1-120) min, (4) Initial Concentration (*IC*) of heavy metals (5-200) mg/L, and (5) Removal Percentage (*RP*) as the response are the five factors that control the system. One factor at a time, experiments were planned around a baseline (pH = 5, *MA* = 6.67 g/L, *CT* = 30 min, *IC* = 10 mg/L). Additionally, to assess the adsorption rate and equilibrium behaviour, kinetic analysis was performed by adjusting *CT* at constant *IC* = 5 mg/L and *MA* = 6.67 g/L. To ascertain the effects of the parameters, each metal system was evaluated in these controlled settings. The dataset consists of 66 adsorption test results, corresponding to 66 records with five input variables and one output variable. Consistency of dataset and nonlinear adsorption behaviour provides a strong basis for statistical modelling, *ML* prediction, kinetic evaluation, and optimisation using metaheuristic and uncertainty analyses in the *ES* that will be outlined below.

Statistical analysis

The statistical analysis in this study was methodically divided into four phases. The first step was data pre-processing for four parameters (pH, *MA*, *CT*, *IC*) as standardising input variables using z-score normalisation, detecting outliers using the Median Absolute Deviation (*MAD*) [27] approach. Second, the distribution of the data was summarised by computing descriptive statistical metrics as mean, standard deviation, quartiles, skewness, and kurtosis. Third, normalised Mutual Information (*MI*) [28] analysis was used to quantify inter-variable interdependence. Lastly, Principal Component Analysis (*PCA*) [29] was used to visualise patterns and reduce dimensionality. MATLAB R2019b was used to carry out all calculations and visualisations.

ANN-GA model structure

Figure 2 demonstrates the model structure for predicting the removal percentage (*RP*) of three heavy metal ions by *ANN* and maximising the *RP*s by *GA*.

Input parameters for creating the *ANN* include Metal type, pH, *MA*, *CT*, and *IC* to predict the *RP* of Pb^{2+}, Co^{2+}, and Mn^{2+} ions. Two hidden layers, each with 10 and 12 neurons, were used with the improved Levenberg-Marquardt training algorithm, or "trainlm" [30]. To guarantee strong generalisation, the dataset was split at random into 70 % for training, 15 % for validation, and 15 % for testing. The output neuron's activation function was set to linear, and the hidden layers' to tangent-sigmoid [30]. Iterative backpropagation was used to adjust the model parameters until the Mean Squared Error (*MSE*) was less than $1 \cdot 10^{-5}$. In this model, the cost function minimises the gap between *ANN*-predicted removal and the 100 % target, allowing *GA* to adjust input factors to maximise adsorption efficiency for each metal ion.

After developing the *ANN*, a *GA* [31] was applied to maximise *RP* by optimising the input variables within their physical ranges. The trained *ANN* was used as a surrogate model during the optimisation process. *GA* had a population of 100, a crossover rate of 0.8, 50 generations, and 10 elites. In this study, mutation was implemented using the default Gaussian mutation operator, which perturbs each decision variable by adding zero-mean

normally distributed noise, with variance controlled by the scale, shrink, and initial population range parameters to preserve diversity and avoid premature convergence [32]. The integrated *ANN-GA* framework [33] autonomously identified optimal operating conditions, ensuring low error and high predictive accuracy across all metal systems. Stochastic uncertainty quantification over the *ANN-GA* optimised adsorption response is carried out *via* the *MC* approach [34]. *MC* simulations (2000 iterations per ion) randomly perturb these ideal parameters within ±5 % to provide probabilistic response distributions once the *ANN* has been trained and the *GA* has identified the best process conditions for each metal ion (Pb^{2+}, Co^{2+}, and Mn^{2+}). In the MC analysis, metal type, defined as a categorical variable (1 = Pb^{2+}, 2 = Co^{2+}, 3 = Mn^{2+}), is fixed within each *MC* run and is determined separately in an outer loop, not treated as a stochastic variable. Statistical descriptors, including mean (*AVG*), standard deviation (*SD*), Coefficient of Variation (*CV*), and (95-99) % Confidence Intervals (*CI*), are produced by recalculating the predicted *RP* using the trained *ANN* model in each iteration. By combining *MC*-driven uncertainty propagation, *GA*-based deterministic optimisation, and *ANN* predictive mapping, the framework allows for the assessment of model robustness and sensitivity to experimental modifications *via* visual dashboards such as *PDF* (Probability Density Function), *CDF* (Cumulative Distribution Function), and box plots. Note that all the declared computations were coded and run in MATLAB 2019b.

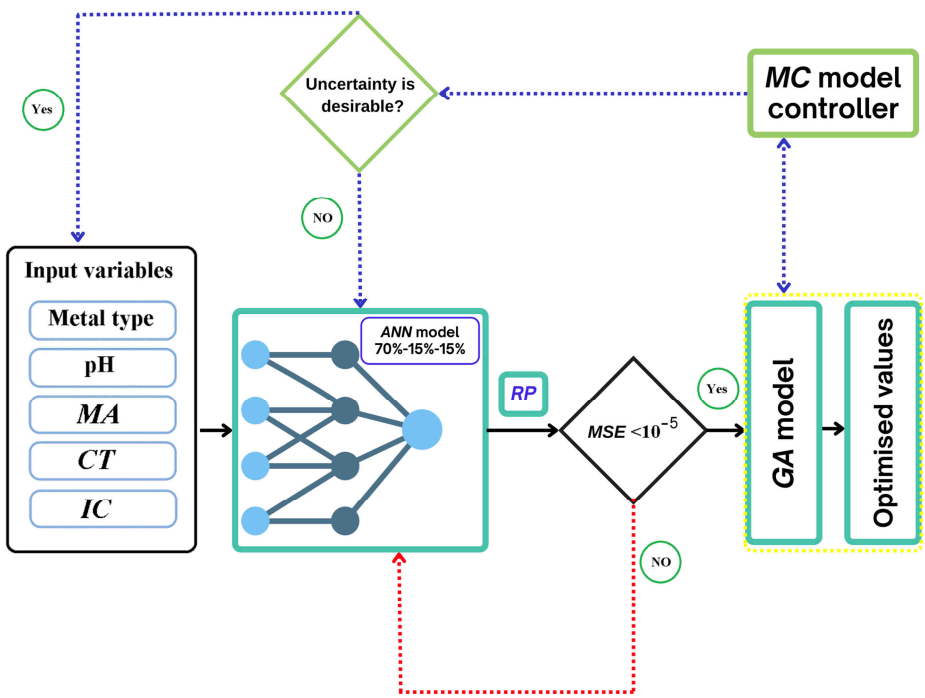

Fig. 2. The structure of *ANN-GA* model in the present study, Condition: *ANN*: Two hidden layers (10, 12 neurons); trainlm algorithm; tansig-hidden, linear-output; *MSE* < $1 \cdot 10^{-5}$; split training: 70 % - testing: 15 % - validation: 15 % and *GA*: Pop 100; crossover 0.8; 50 generations; 10 elites; maximised *RP* → 100 % *via* optimised inputs

Expert system structure

An *ES* for intelligent control of metal ion removal in an industrial water treatment plant is formed by the implemented MATLAB R2019b software. To anticipate *RP*, it incorporates a feed-forward *ANN* trained on past process data, including Metal type, pH, *MA*, *CT*, and *IC*. To attain maximum *RP* for Pb^{2+}, Co^{2+}, and Mn^{2+}, these parameters are refined by *GA* optimisation. To simulate actual water treatment plant conditions, the system creates 200 synthetic sensor-based test datasets [35], allowing for online prediction and adaptive learning.

The synthetic online sensor dataset was generated within the experimentally validated operating domain by defining the input vector $x = [m,\mathrm{pH},MA,CT,IC]$, where the metal type $m \in \{1,2,3\}$ was treated as a fixed categorical variable and continuous parameters were sampled from bounded uniform distributions $\sim U(x_{i\text{-}min},x_{i\text{-}max})$. Sensor uncertainty was emulated *via* multiplicative noise $x_i' = x_i(1+\epsilon_i)$, with $\epsilon_i \sim U(-0.02,0.02)$ followed by range projection. Subsequently, *MC* analysis perturbed the *ANN-GA* optimised parameters within ±5 % over multiple realisations to quantify process-level uncertainty around the optimal operating point. The 2 % simulated sensor uncertainty represents a controlled and reliable measurement regime, while the 5 % *MC* perturbation encompasses broader process and operational variability; thus, the smaller sensor noise is intentionally nested within the larger *MC* uncertainty to reflect the hierarchical nature of measurement and operational uncertainties.

The *ES* assesses operational dependability and model robustness using visual dashboards (response surfaces, Key Performance Indicators: *KPI*s, and process flow) and performance indicators (Coefficient of Determination: R^2, Root Mean Square Error: *RMSE*, and Mean Absolute Error: *MAE*). While further work concentrates on *ES* performance validation under dynamic water treatment scenarios, the structure permits interfacing with sensors for autonomous optimisation.

Results and discussion

At the first stage, the specification of the dataset and available experimental results of Pb^{2+}, Co^{2+}, and Mn^{2+} adsorption onto the surface of *LDC* is analysed. A thorough summary of the features of the input dataset, inter-variable dependencies, and their overall variance structure relative to the *RP* is given in Figure 3.

The dataset was deemed complete, since there were no missing values in any of the response parameters (removal percentage) or input parameters (Metal type, pH, *MA*, *CT*, and *IC*). This validated the data's reliability for subsequent statistical analysis and modelling. Figure 3a shows the Normalised Mutual Information (*NMI*) matrix between the input variables. The off-diagonal *NMI* values remain below 0.12, indicating that each input delivers significantly independent information and confirming weak correlations among variables. A slight correlation (≈ 0.12) is observed between *CT* and *IC* in the adsorption test results. However, the categorical variable metal type exhibits negligible mutual information with all continuous variables, confirming minimal redundancy. Moreover, as metal type is a categorical variable, its low correlation with continuous parameters is expected and does not imply a lack of influence on removal efficiency. Therefore, the inclusion of all predictors in the modelling framework is justified, and the risk of multicollinearity is substantially reduced. Boxplots, which are a valuable tool for visualising central tendency, dispersion, and the existence of high-leverage observations, are used to display the input

variable distributions in Figure 3b. The pH variable has a clear left skew (skew = –2.81, kurtosis = 9.9, median = 5), with a few low extreme values. The *MA* variable exhibits a moderately left-skewed distribution (skew = –1.18, kurtosis = 5.84), with most values clustered around 6.67 g/L and a limited number of high-leverage observations, indicating general consistency with occasional deviations. *CT* displays a broad and right-skewed distribution (skew = 2.08, kurtosis = 6.41), spanning from 10 to 120 min, with 26 high-value influential observations. *IC* demonstrates the most pronounced non-Gaussian behaviour, with an extreme right skew (skew = 3.33, kurtosis = 13.63), a dominant median of 10 mg/L, and nine high-leverage observations up to 200 mg/L, reflecting irregular concentration spikes.

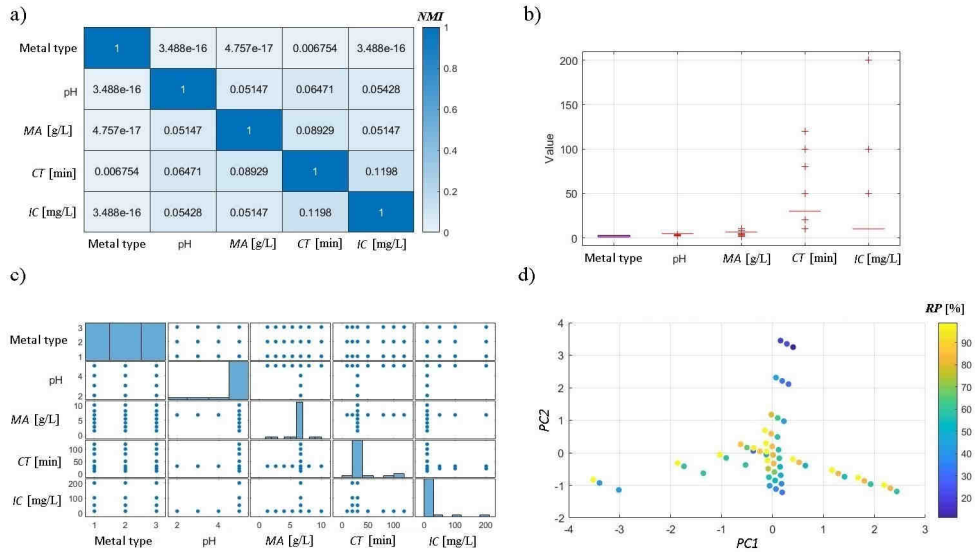

Fig. 3. Exploratory data analysis of input variables as per: a) normalised mutual information matrix according to weak inter-variable dependencies, b) boxplots as per skewed and heavy-tailed distributions with multiple high-leverage observations, c) Scatter matrix based on weak linear relationships among inputs, and d) *PCA* score plot (*PC1* = 23.8 %, *PC2* = 22.1 %) as per nonlinear variance patterns coloured by *RP*

The scatter matrix of input variables is shown in Figure 3c, enabling a visual examination of pairwise correlations. Consistent with the low *NMI* values (see Fig. 3a), the scatter plots exhibit diffuse and weakly structured patterns, confirming the absence of significant linear correlations. While *CT* and *IC* histograms along the diagonal indicate heavy-tailed distributions, Metal type and pH plots' vertical and horizontal bands are the result of their discrete or limited numeric levels. The absence of clear patterns indicates that potential correlations between these characteristics and *RP* are likely nonlinear and influenced by complex interactions rather than simple linear dependencies.

The first two Principal Components (*PC1* and *PC2*) account for 23.8 % and 22.1 % of the total variance, respectively, according to the *PCA* score plot displayed in Figure 3d. Together, *PC1* and *PC2* explain about 45.9 % of the total variance, indicating that nearly half of the dataset variability is represented in the two-dimensional *PCA* space, while the

remaining variance is distributed across higher components. This further confirms the inherent complexity of the adsorption dataset. The combination of discrete (Metal type, pH) and continuous (*MA*, *CT*, *IC*) variables results in a cross-shaped pattern in the score distribution. It is implied that *RP* variation results from a number of interrelated elements rather than a dominant linear trend because the *RP* colour gradient does not correspond linearly with either component.

In general, Figure 3 shows that the dataset is statistically complete, with skewed and heavy-tailed distributions and low correlation among predictors. The nonlinear structure indicates that advanced methods such as *ML* and *GA* or their integrations are suitable for predicting RP and supporting automated optimisation of the adsorption process.

In accordance with Zhao et al. [36], who highlighted that heavy metal adsorption systems display multivariate yet weakly coupled nonlinearities prior to interaction effects predominating, enabling ML models to isolate governing parameters, the weak mutual information among input variables suggests minimal collinearity. Therefore, under these conditions, the application of ML models is essential for addressing this type of problem, as adopted in this study.

Figure 4 presents the *ANN-GA* results, covering model diagnostics, optimisation outcomes, and prediction performance. With dispersion only rising at the highest removal levels, Figure 4a demonstrates a close parity between actual and predicted *RP* for all three metals (R^2 = 0.908, *RMSE* = 7.43 %, *MAE* = 5.04 %). As shown in Figure 4g, rapid error reduction occurs within approximately 5-8 epochs, and the stable test curve indicates minimal overfitting and good generalisation. Consistent with the heavy-tailed inputs previously noted, the residuals in Figure 4h exhibit a small mean bias (mean = 0.49), approximately homoscedastic variance, and are largely limited within ±2σ (σ = 7.47), with a few pronounced deviations observed at high *RP* values (> 50 %).

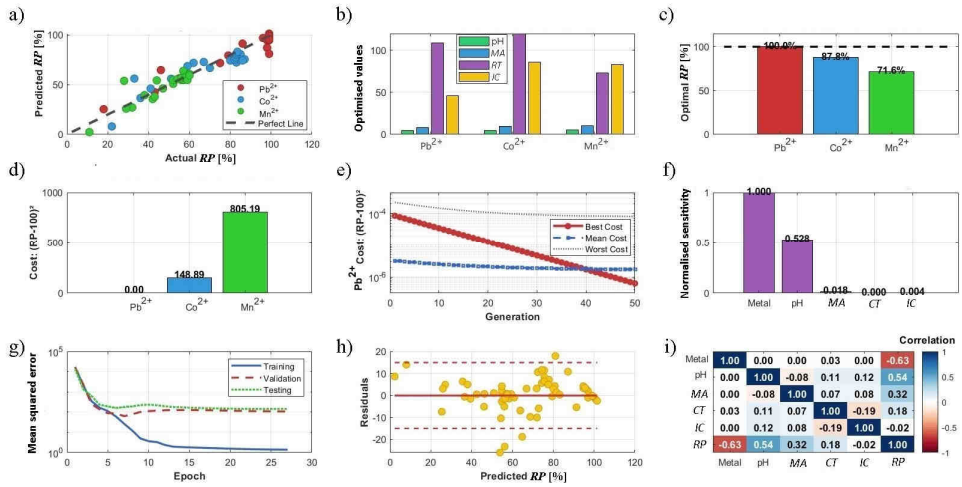

Fig. 4. *ANN-GA* outcomes for ion removal based on: a) actual vs. predicted RP values, b) *GA* settings and optimal value suggestions for all input parameters (pH, *MA*, *CT*, and *IC*), c) maximum performance of *RP* per ion, d) cost function values per ion, e) convergence to best cost by 50 generations, f) sensitivity analysis of input variables, g) learning curves as per stable generalisation, h) residuals values, and i) Pearson correlation matrix of input/output parameters

The *GA* optimisation is reported in Figures 4b-e. Over 50 generations, the *GA* gradually reduces the best objective function (for instance, Pb^{2+}: Fig. 4e), keeping the best and mean costs apart and preventing protracted stalls, which shows ongoing exploitation with some population variety. In Figure 4b, high pH (near the top bound), *MA* ≈ (8.26-10) g/L, specific *IC* ≈ (46.2-86.2) mg/L, and metal-specific *CT* (high for Pb^{2+}/Co^{2+} and lower for Mn^{2+}) are the clustered optimal operating points. As shown in Figures 4c and 4d, Mn^{2+} reaches a maximum removal of 71.6 % and exhibits the highest optimisation cost function value (805.19), compared with Pb^{2+}, which achieves 100 % removal with zero cost, and Co^{2+}, which attains 87.8 % removal with a cost of 148.89.

These results indicate that Mn^{2+} requires process intensification or an expanded design space, as it is inherently more difficult to remove under the studied conditions. The results of the optimisation for critical parameters *vs. RP* are demonstrated in Table 1.

Table 1

The results of *ANN-GA* model optimisation based on experimental input data

Metal ion	***IC* [mg/L]**	**pH [-]**	***MA* [g/L]**	***CT* [min]**	***RP* [%]**
Pb^{2+}	46.2	4.8	8.26	109	100
Co^{2+}	86.2	5	9.99	120	87.8
Mn^{2+}	82.9	5	10	73	71.62

The interpretation of the model results in Figures 4f and 4i is the same. According to the normalised sensitivity analysis, metal type emerges as the dominant control variable (1.000), followed by pH (0.528) with a strong secondary influence, while *MA* (0.018), *CT* (≈ 0), and *IC* (0.004) exhibit very limited direct sensitivity. Moreover, Figure 4i presents the Pearson correlation matrix, showing the relationships between *RP* and the other heavy metal adsorption variables. Most notably, *RP* exhibits a strong negative correlation with metal type (–0.63), indicating that as the metal type defined number increases (from Pb^{2+} to Mn^{2+}), *RP* values tend to decrease substantially. Conversely, *RP* demonstrates a moderate positive correlation with pH (0.54), suggesting that higher pH levels are associated with elevated *RP* values. Additionally, *RP* shows a weak to moderate positive relationship with *MA* (0.32), while *CT* displays only a minimal correlation (0.18). The *IC* parameter appears nearly independent of *RP*, with a correlation coefficient of –0.02. Together, these diagnostics are used to support the *ANN* as a reliable surrogate model for *GA*-based search, and a practical strategy is suggested in which pH control is prioritised, *MA* is adjusted as a secondary lever, and *CT* and *IC* are treated as lower-order constraints.

The *ANN-GA* hybrid approach has demonstrated strong predictive capabilities across various adsorption systems. Fan et al. [37] achieved R^2 = 0.99 for Cd^{2+} removal using Reduced Graphene Oxide-Supported Nanoscale Zero-Valent Iron (nZVI/rGO) composites, while Halder et al. [38] reported R^2 = 0.991 for Cr^{6+} adsorption optimisation, and Mandal et al. [39] obtained R^2 = 0.975 for As^{3+} removal. The current study's R^2 = 0.908, while slightly lower, is attributable to the inherent variability of waste-derived adsorbents (*LDC*) compared to engineered materials, and single-metal batch experiments. Importantly, the current study extends beyond prediction accuracy to integrate *GA* optimisation and *MC* uncertainty quantification, providing operational robustness metrics (*CV* values) absent in prior *ANN*-only approaches. The identification of pH as dominant variable aligns with Mandal et al. [39] findings, confirming the reliability of the sensitivity analysis despite the moderate R^2 value.

GA convergence across metals is compared in Figure 5a-c. For Pb^{2+} (Fig. 5a), the best-cost value decreases rapidly from ~10^{-4} to less than 10^{-6} (≈ 99.3 % reduction in the cost function relative to the initial *GA* baseline) with a reduction of best-mean gap. Moreover, for Co^{2+} (Fig. 5b), the best-cost decreases nearly exponentially from ~ more than $2 \cdot 10^3$ to 148.89 (≈ 94.3 % improvement), indicating the stable convergence. Finally, for Mn^{2+} (Fig. 5c), the best cost remains high (805.19) despite a 47.5 % improvement, indicating a more difficult optimisation landscape.

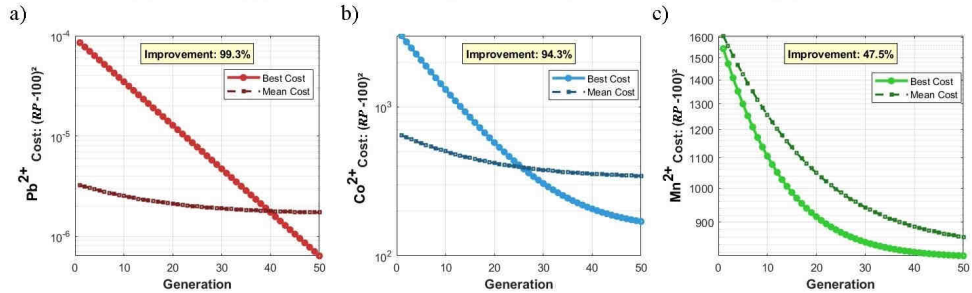

Fig. 5. *GA* convergence by metal: a) Pb^{2+}, b) Co^{2+} and c) Mn^{2+}. *GA* conditions: population size: 100, 50 generations, elite count: 10, crossover fraction: 0.80, fitness based on squared deviation of removal percentage from 100 %

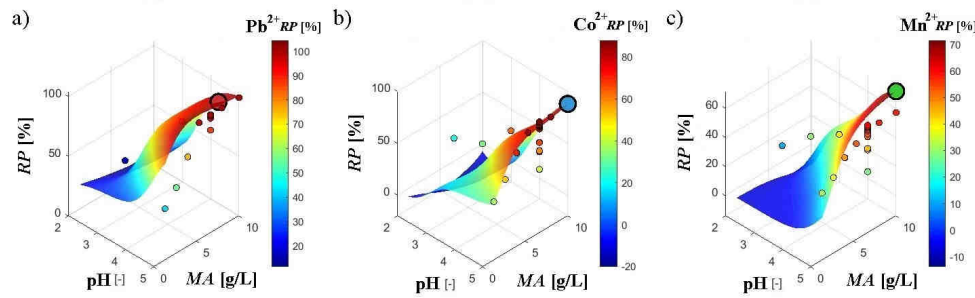

Fig. 6. Response surfaces (*RP vs.* pH, *MA*): a) Pb^{2+} (*CT*: 109 min, *IC*: 46.2 mg/L) and b) Co^{2+} (*CT*: 120 min, *IC*: 86.2 mg/L), and c) Mn^{2+} (*CT*: 73 min, *IC*: 82.9 mg/L) as per *ANN-GA* simulations, *GA* conditions: population size: 100, 50 generations, elite count: 10, crossover fraction: 0.80, fitness based on squared deviation of removal percentage from 100 %

For each Metal type at different specific *CT* and *IC*, Figure 6 plots the *ANN-GA* response surfaces of *RP* against pH and *MA*. As *MA* approaches approximately (6.67-10) g/L, *RP* increases markedly, with improvements near the lower acidity boundary (pH ≈ 5) further enhanced by pH effects. At high *MA* and pH, Pb^{2+} shows near-complete removal across a broad region (Fig. 6a). Moreover, Co^{2+} exhibits a similar trend but with different pH-*MA* interaction effects (Fig. 6b). Besides, Mn^{2+} displays a smoother response and a lower removal plateau of about 70 % (Fig. 6c), indicating lower adsorption efficiency. Pb^{2+} has a lower hydration energy and acts as a softer Lewis acid, which favours strong inner-sphere complexation with alkaline *LDC* surface sites and permits incipient precipitation as $Pb(OH)_2$/basic carbonates at high pH [25]. This superiority is mechanistically feasible. These findings align with those of Macena et al. [40], who

determined that variations in adsorption affinity among heavy metals are affected mainly by ionic softness, hydration state, and the extent of complexation with surface functional groups.

The *ANN-GA* framework's model-based outputs for single factors vs. *RP*, are shown in Figures 7a-d. The effects of pH, *MA*, *CT*, and *IC* on *RP* collectively reveal a consistent adsorption hierarchy among the metal ions. Increasing pH enhances *RP* for Pb^{2+} and Co^{2+}, leading to high removal efficiencies at the upper pH range, whereas Mn^{2+} exhibits a weaker and more gradual response, with moderate removal efficiency at higher pH. In parallel, increasing *MA* strongly promotes *RP* for all metals, with Pb^{2+} and Co^{2+} showing a sharp rise, while Mn^{2+} requires higher *MA* values to achieve comparable performance. Prolonged *CT* has a limited additional effect, rapidly driving Pb^{2+} and Co^{2+} toward early saturation, whereas Mn^{2+} remains partially kinetically constrained. Conversely, increasing *IC* reduces *RP* due to active site saturation, with this inhibitory effect being most pronounced for Mn^{2+} because of its weaker surface affinity. From the standpoint of control systems, the main variables that should be changed (high loop gain) are pH and *MA*. Then, *CT* should be adjusted for each metal (longer for Co^{2+}). The outcomes illustrated in Figure 7d indicate that *IC* has the lowest influence on *RP* according to the *ANN-GA* model, exhibits an inverse relationship with *RP*, and, due to its fluctuations, should be specifically controlled for Co^{2+} at the optimal values reported in Table 1.

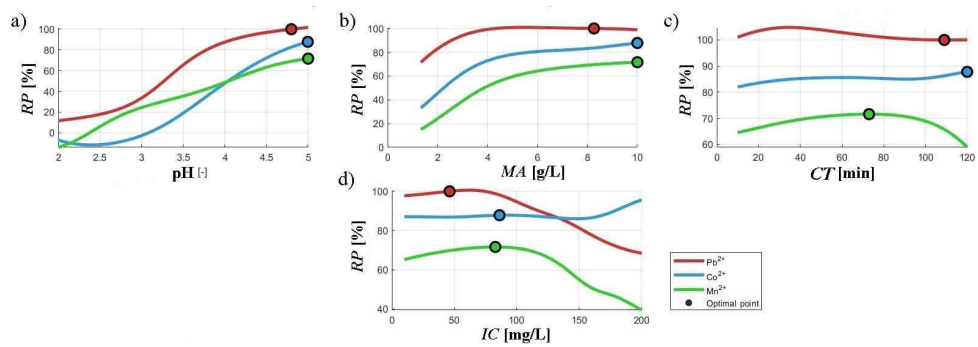

Fig. 7. *ANN-GA* response curves for Pb^{2+}, Co^{2+}, Mn^{2+} as per: a) pH *vs. RP*, b) *MA vs. RP*; c) *CT vs. RP*; d) *IC vs. RP*, *GA* conditions: population size: 100, 50 generations, elite count: 10, crossover fraction: 0.80, fitness based on squared deviation of removal percentage from 100 %. Note: In each plot, the remaining factors are fixed at their optimal values as listed in Table 1

Huang et al. [41] explained that precipitation, surface complexation, and ion exchange within the C–S–H and ettringite phases are necessary for heavy metal stabilisation in waste-based matrices, and the *GA* optimisation results following *ANN* prediction in this study are in good agreement with their findings. Co^{2+} and Mn^{2+} showed lesser fixation because they were present in more soluble forms, such as $MnSO_4 \cdot 2H_2O$, but Pb^{2+} demonstrated the highest stability through the development of insoluble hydroxide and phosphate precipitates ($Pb(OH)_2$, $Pb_3(PO_4)_2$). Stronger adsorption and precipitation under alkaline conditions are confirmed by the observed pH-dependent enhancement in removal, which is in line with Huang's [41] solidification mechanisms.

Figure 8 quantifies the reliability of the optimal operating rules under input variability and complements the preceding *ANN-GA* results. *MC* uncertainty analysis of the *ANN-GA* model is reported in all panels.

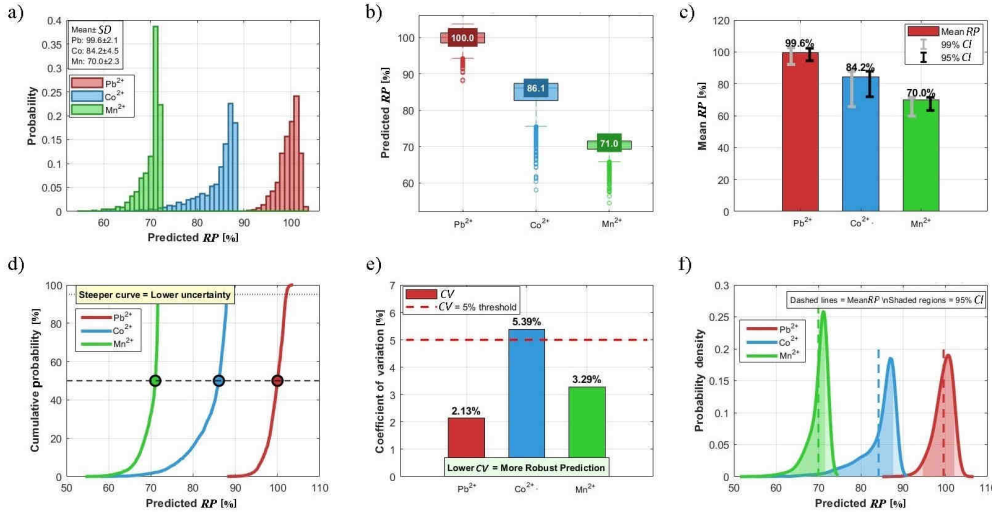

Fig. 8. *ANN-GA-MC* (2,000 runs) uncertainty: a) *RP* distributions, b) boxplots of *MC* analysis, c) means with 95/99 % Confidence Intervals (*CI*s), d) steep *CDF*s indicate robustness (Pb^{2+}, Co^{2+}), e) *CV*s in the three metals adsorption onto *LDC*, and f) *PDF*s to set control margins, *MC* Conditions: 2000 runs, ±5 % perturbation of pH, *MA*, *CT*, *IC*, *ANN*-based *RP* uncertainty

After 2000 MC cycles at GA-recommended settings (Fig. 8a), uncertainty quantification reveals metal-specific variability patterns. By absolute standard deviation, Pb^{2+} (SD = 2.1 %) shows the lowest variability, followed by Mn^{2+} (SD = 2.3 %) and Co^{2+} (SD = 4.5 %). In the probability density histograms, Mn^{2+} exhibits the tallest peak due to its untruncated distribution around 70 %, while Pb^{2+}'s distribution near the physical 100 % limit appears broader due to edge effects, and Co^{2+} displays the widest spread centered at 84.2 %.

Boxplots of the *MC*-predicted *RP* values are shown in Figure 8b. Pb^{2+} confirms modest dispersion and consistent performance with a narrow interquartile range and few deviant values. Co^{2+} shows significant variability under uncertainty with a large interquartile range and several low-value outliers. Mn^{2+} exhibits a modest spread, much narrower than Co^{2+} but bigger than Pb^{2+}, indicating regulated but not insignificant variability. Further, Figure 8c compares the *MC* mean *RP* values with their corresponding 95 % *CI*. Pb^{2+} achieves a mean *RP* of 99.6 %, with a 95 % *CI* of [94.51 %, 102.31 %], confirming near-complete and highly reliable removal. Co^{2+} reaches a mean *RP* of 84.2 %, with a wider 95 % *CI* of [71.87 %, 87.94 %], indicating reduced robustness. Mn^{2+} exhibits a mean *RP* of 70.00 %, bounded by a narrower 95 % *CI* of [63.37 %, 71.62 %], reflecting moderate stability around its optimal value.

The *CDFs* of *RP* are shown in Figure 8d. The steep slope of the Pb^{2+} *CDF* indicates a high probability of achieving *RP* values close to the optimum with minimal uncertainty. Besides, the more gradual slope observed for Co^{2+} reflects greater variability and a higher

likelihood of deviation from ideal performance. The Mn^{2+} CDF lies between these two extremes, indicating moderate robustness and resilience. Moreover, each metal ion's *CV* is shown in Figure 8e. The most reliable prediction is Pb^{2+}, which shows the least fluctuation (*CV* = 2.13 %). The moderately stable system under stochastic perturbations is Mn^{2+}, which exhibits moderate variability (*CV* = 3.29 %), but Co^{2+} surpasses the 5 % robustness barrier (*CV* = 5.39 %) based on the study of González-Fernández et al. [42]. The *PDFs* of *RP* are shown in Figure 8f, with shaded areas denoting the 95 % confidence intervals and dashed lines denoting the *MC* mean. Strong dependability and narrow control margins are confirmed by the crisp, high-density peak that Pb^{2+} displays. Because of its flatter and wider density profile, Co^{2+} needs more cautious operational management. Once more, Mn^{2+} exhibits intermediate behaviour, with reasonable uncertainty boundaries and a moderately concentrated density.

To assess parameter sensitivity in micellar-enhanced ultrafiltration, Lin et al.'s [43] *MC-ANN* model employed 1000 stochastic iterations. It achieved over 99 % metal rejection and identified pH and surfactant ratio as the dominating parameters with the least amount of model uncertainty. Similarly, to evaluate resilience and regulate variability, the current *ANN-GA-MC* paradigm combines evolutionary optimisation with probabilistic *MC* simulations.

The MATLAB-based system illustrates how *ML*, optimisation, and sensor-based analytics are integrated under the Industry 4.0 paradigm in the simulated operation of the *ES* within an industrial water treatment plant. The *ES* turns static adsorption modelling into a dynamic decision-support environment that can intelligently govern processes, as seen in Figure 9 as the online dashboard output. The average *RP* for Pb^{2+}, Co^{2+}, and Mn^{2+} ions is continuously forecasted on the real-time control dashboard, which is shown in the upper panel. Across 200 synthetic test scenarios with varied operational conditions, Pb^{2+} exhibits the highest average RP (69.4 %), followed by Co^{2+} (63 %) and Mn^{2+} (47 %), while GA-optimised conditions achieve maximum removals of 100 % (Pb^{2+}), 87.8 % (Co^{2+}), and 71.6 % (Mn^{2+}).

The simulation's varied operational variability is validated by the pH and sorbent mass distributions obtained from 200 synthetic sensor-based test datasets. Time and concentration are secondary under optimised regimes, while pH and sorbent mass dominate process sensitivity, as seen by the ideal parameter heatmap. The capacity of the system to generalise predictions under industrial noise and uncertainty is demonstrated by the *ANN* training and validation curves (R^2 = 0.993), which show consistent convergence with little overfitting. In this study, R^2 = 0.908 represents the *ANN* performance on training, validation, and testing, while R^2 = 0.993 is obtained within the *ES* using simulated sensor-based data (just training and validation). The observed difference ($\Delta R^2 \approx 0.085$) reflects the exclusion of unseen test data and the resulting evaluation under more stable, operator-controlled conditions. This difference does not imply a change in model structure, but rather the performance of the same ANN when assessed using training and validation data only.

From a smart operational perspective, the *ES* integrates predictive analytics with autonomous optimisation loops. The *GA* iteratively refines operational setpoints to maximise the RP of Pb^{2+}, Co^{2+}, and Mn^{2+}, with *ANN* outputs continuously integrated into the GA-based control logic. These results indicate that the system can adaptively regulate treatment parameters, maintaining process efficiency despite fluctuating influent quality.

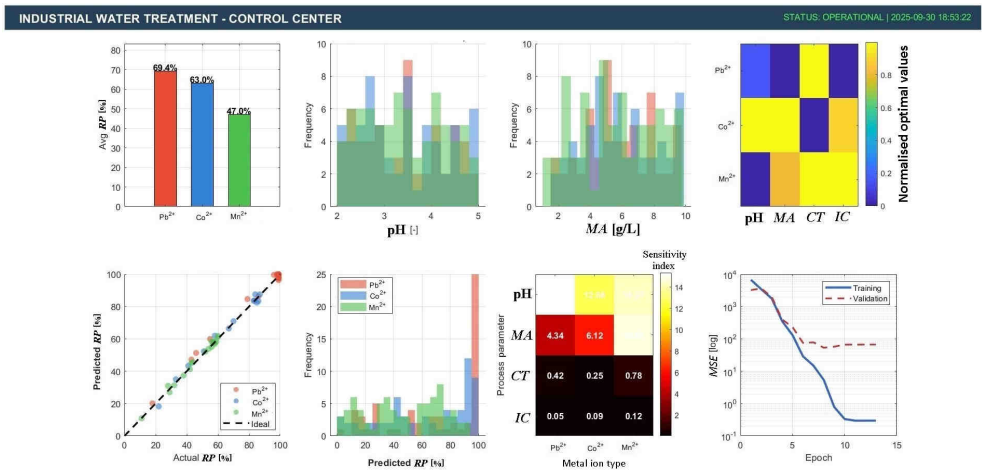

Fig. 9. Industrial water treatment control centre dashboard of the developed *ES* as per sensor-based data processing, *ANN-GA* predictive modelling, parameter optimisation, and intelligent monitoring within an Industry 4.0 operational framework

Figure 10 presents the online dashboard output, illustrating the optimisation outcomes of the *ES* through 3D response surface plots and contour maps for each metal ion. The surfaces visualise the nonlinear interplay between pH and *MA* on *RP*, illustrating that performance enhancement is primarily achieved within the high-pH, high-*MA* domain. The overlaid optimal points indicate the system's ability to autonomously discover the most efficient zones for operation.

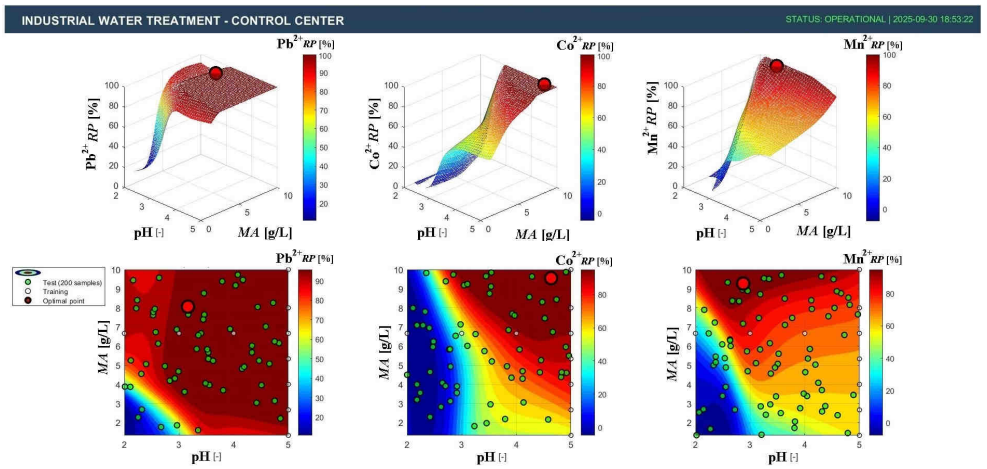

Fig. 10. Digital twin dashboard according to *ANN-GA*-based optimisation analysis, response surfaces, and optimal operational zones for Pb^{2+}, Co^{2+}, and Mn^{2+} adsorption in industrial level analysis

Using an *ANN*, *RF*, Radial Basis Function kernel, and Adaptive Neuro-Fuzzy Inference System (*ANFIS*), Pathania et al. [44] created an online *AI*-based wastewater monitoring system that predicts pollutant adsorption in real time. However, their approach focused on prediction without optimisation. Wilson et al. [45] created a real-time biosorption monitoring system from an automation standpoint by combining an *ANN* model with an electronic tongue and a flow-injection potentiometric setup to assess transient signals from ion-selective sensors. This setup made it possible to identify several metals at once and partially automate the monitoring procedure. In order to facilitate optimisation and decision-making inside an Industry 4.0, the current study combines *ANN*, *GA*, and *MC* to advance automation.

By coupling *ANN-GA* predictive modelling with *MC*-based uncertainty analysis, the developed *ES* not only predicts and optimises removal efficiencies for Pb^{2+}, Co^{2+}, and Mn^{2+} but also quantifies operational robustness under realistic variations. The current approach changes adsorption modelling from a static optimisation or data-driven prediction tool into a decision-support system capable of real-time process control. This advancement aligns with the emerging concept of Virtual Laboratories [46], enabling digital experimentation, model validation, and process optimisation in simulated environments. Consequently, it establishes a scalable digital twin framework for sustainable water treatment systems. This could make it easier to connect with Internet of Things (*IoT*)-based sensing and real-time industrial automation in the future.

Conclusion

In this study, the *ANN-GA* framework predicted optimal removal efficiencies of 100 % for Pb^{2+}, 87.8 % for Co^{2+}, and 71.62 % for Mn^{2+}, with predictive accuracy of R^2 = 0.908 and *RMSE* = 7.43 %. *MC* analysis confirmed high operational robustness for Pb^{2+} (*CV* = 2.13 %) and Mn^{2+} (*CV* = 3.29 %), while Co^{2+} showed higher variability (*CV* = 5.39 %). By combining automation, uncertainty analysis, and process sustainability, the *ES* offers managerial decision assistance beyond technical optimisation, facilitating data-driven resource management and operational resilience in water treatment systems. By transforming construction and demolition waste into high-value functional adsorbents, the framework reduces reliance on virgin materials, reinforces circular resource utilisation, and contributes to UN SDGs 6 (Clean Water), 9 (Industry Innovation), and 12 (Responsible Consumption). In order to support sustainable process automation and informed policy development for environmental protection, the methodology converts static experimental insights into an eco-efficient digital twin framework. To improve sustainability, scalability, and circular economy integration in industrial water treatment, future research might expand the *ES* to dynamic multi-metal and real wastewater conditions, incorporate IoT-based real-time monitoring, and investigate hybrid organic waste-*LDC* composites.

Acknowledgements

This work was supported by the European Union's HORIZON EUROPE WIDERA 2021 program under the SURRI project, Grant Agreement No 101079345. Stanisław Wacławek acknowledges the support of the Ministry of Education, Youth and Sports under the ERC CZ program project "Hydrated electron: the alchemist stone of water treatment CZ" (LL2501) and the project "Reducing Heavy Metal Pollution in Agriculture - Metallica" (8J24AT037).

References

[1] Jin X, Tong X, Hua S, Xu Y. Ecological and health risk assessment of soil heavy metal contamination along National Highway 107 in China. Ecol Chem Eng S. 2024;31(2):155-75. DOI: 10.2478/eces-2024-0011.

[2] Zein R, Wulandari S, Ramadhani P, Deswati D. Utilisation of shrimp shell as a low-cost biosorbent for the adsorption of methylene blue dyes. Ecol Chem Eng S. 2024;31(1):63-73. DOI: 10.2478/eces-2024-0005.

[3] Prasad MNV, Elchuri SV. Environmental contaminants of emerging concern: Occurrence and remediation. Chem Didact Ecol Metrol. 2023;28(1-2):57-77. DOI: 10.2478/cdem-2023-0004.

[4] Wacławek M, Świsłowski P, Rajfur M. The biological monitoring as a source of information on environmental pollution with heavy metals. Chem Didact Ecol Metrol. 2022;27(1-2):53-78. DOI: 10.2478/cdem-2022-0006.

[5] Kozłowski R, Strzyż M. Heavy metals accumulation in silver fir needles in Swietokrzyski National Park. Chem Didact Ecol Metrol. 2021;26(1-2):65-72. DOI: 10.2478/cdem-2021-0005.

[6] Dąbek L, Picheta-Oleś A, Szeląg B, Szulżyk-Cieplak J, Łagód G. Modeling and optimization of pollutants removal during simultaneous adsorption onto activated carbon with advanced oxidation in aqueous environment. Materials. 2020;13(19):4220. DOI: 10.3390/ma13194220.

[7] Kujawska J, Wojtaś E, Zaburko J, Kamińska I, Czerpak J, Jamka K, et al. Concentration and risk assessment of metals in snow cover monitoring in urban and rural areas. Ann Agric Environ Med. 2024;31(2):205-11. DOI: 10.26444/aaem/190317.

[8] Kujawska J, Duda-Saternus S, Szulżyk-Cieplak J, Zaburko J, Piłat-Rożek M, Jamka K, et al. Comparison of leaching behaviour of heavy metals from sediments sampled in sewer systems - environmental and public health aspect. Ann Agric Environ Med. 2023;30(4):677-84. DOI: 10.26444/aaem/175553.

[9] Duda-Saternus S, Kujawska J, Wojtaś E, Kozłowska A, Jamka K, Szeląg B, et al. A simplified method for determining potential heavy metal leached from sediments ofstormwater and combined sewer systems - importance for public health. Ann Agric Environ Med. 2023;30(3):455-61. DOI: 10.26444/aaem/170099.

[10] Qasem NAA, Mohammed RH, Lawal DU. Removal of heavy metal ions from wastewater: a comprehensive and critical review. Npj Clean Water. 2021;4(1):36. DOI: 10.1038/s41545-021-00127-0.

[11] Eftekhari M, Gheibi M, Azizi-Toupkanloo H, Hossein-Abadi Z, Khraisheh M, Fathollahi-Fard AM, et al. Statistical optimization, soft computing prediction, mechanistic and empirical evaluation for fundamental appraisal of copper, lead and malachite green adsorption. J Ind Inf Integr. 2021;23:100219. DOI: 10.1016/j.jii.2021.100219.

[12] Fiyadh SS, Alardhi SM, Omar MA, Aljumaily MM, Saadi MAA, Fayaed SS, et al. A comprehensive review on modelling the adsorption process for heavy metal removal from waste water using artificial neural network technique. Heliyon. 2023;9(4). DOI: 10.1016/j.heliyon.2023.e15455.

[13] González Costa JJ, Reigosa MJ, Matías JM, Covelo EF. Soil Cd, Cr, Cu, Ni, Pb and Zn sorption and retention models using SVM: Variable selection and competitive model. Sci Total Environ. 2017;593-594:508-22. DOI: 10.1016/j.scitotenv.2017.03.195.

[14] Moradpour S, Entezari M, Ayoubi S, Karimi A, Naimi S. Digital exploration of selected heavy metals using Random Forest and a set of environmental covariates at the watershed scale. J Hazard Mater. 2023;455:131609. DOI: 10.1016/j.jhazmat.2023.131609.

[15] Liang C, Zhang Z, Li Y, Wang Y, He M, Xia F, et al. Simulation, prediction and optimization for synthesis and heavy metals adsorption of schwertmannite by machine learning. Environ Res. 2025;265:120471. DOI: 10.1016/j.envres.2024.120471.

[16] Leng L, Zheng H, Shen T, Wu Z, Xiong T, Liu S, et al. Engineering biochar from biomass pyrolysis for effective adsorption of heavy metal: An innovative machine learning approach. Sep Purif Technol. 2025;361:131592. DOI: 10.1016/j.seppur.2025.131592.

[17] Wang J, Liu X, Li W, Tu Y, Deng H, Du J. Deciphering heavy metal adsorption capacity of soil based on its physicochemical properties and adsorption reaction time using machine learning. J Environ Chem Eng. 2025;13(3):116913. DOI: 10.1016/j.jece.2025.116913.

[18] Yaseen ZM, Alhalimi FL. Heavy metal adsorption efficiency prediction using biochar properties: a comparative analysis for ensemble machine learning models. Sci Rep. 2025;15(1):13434. DOI: 10.1038/s41598-025-96271-5.

[19] Han Y, Dai W, Zhou L, Guo L, Liu M, Wang D, et al. Predicting the adsorption capacity of geopolymers for heavy metals in solution based on machine learning. J Environ Chem Eng. 2025;13(2):115978. DOI: 10.1016/j.jece.2025.115978.

[20] Hassan R, Behtouei Z, Baghban A. Advanced machine learning for precise prediction of biochar's heavy metal sorption efficiency. J Ha□ard Mater Adv. 2025;18:100739. DOI: 10.1016/j.hazadv.2025.100739.

[21] Tank S, Pandey M, Rath JJ, Bandyopadhyay M. Base modified mesoporous silica adsorbent for heavy metal adsorption: Optimization of adsorption efficiency with machine learning algorithms. Hybrid Adv. 2025;10:100489. DOI: 10.1016/j.hybadv.2025.100489.
[22] Xu M, Zhang L, Yuan L, Ji C, Zhang Y, Kong D, et al. Machine learning-assisted adsorption capacity prediction of ion exchange or chelate resin for heavy metals in aqueous solutions: External validation via multi-factor experiments. Sep Purif Technol. 2025;368:133019. DOI: 10.1016/j.seppur.2025.133019.
[23] Wang Z, Wang B, Liu Q, Huo X, Chang T, Sun J, et al. Predicting heavy metals adsorption on microplastics and unraveling the adsorption mechanism with machine learning methods. Surf Interfaces. 2025;72:107101. DOI: 10.1016/j.surfin.2025.107101.
[24] Gheibi M, Wacławek S, Leo CP, Sadr S, Behzadian K. Dynamic modelling, simulation, and sensitive analysis of lead removal in a fixed-bed adsorption column using waste-based materials. IOP Conf Ser Earth Environ Sci. 2024;1368(1):012009. DOI: 10.1088/1755-1315/1368/1/012009.
[25] Gheibi M, Masoomi SR, Eftekhari M, Akrami M, Palušák M, Silvestri D, et al. Heavy metals adsorption using CDW adsorbents: A sustainable path for water purification. J Hazard Mater Adv. 2025;20:100883. DOI: 10.1016/j.hazadv.2025.100883.
[26] Michalak A, Świsłowski P, Rajfur M. The assessment of heavy metal contamination of the cultivated soils in the Odra River Floodplain. Chem Didact Ecol Metrol. 2021;26(1-2):55-64. DOI: 10.2478/cdem-2021-0004.
[27] Rousseeuw PJ, Croux C. Alternatives to the median absolute deviation. J Am Stat Assoc. 1993;88(424):1273-83. DOI: 10.1080/01621459.1993.10476408.
[28] Veyrat-Charvillon N, Standaert FX. Mutual information analysis: How, when and why? In: Clavier C, Gaj K, editors. Cryptographic Hardware and Embedded Systems - CHES 2009. Berlin, Heidelberg: Springer; 2009; 429-43. DOI: 10.1007/978-3-642-04138-9_30.
[29] Al-Degs YS, Abu-El-Halawa R, Abu-Alrub SS. Analyzing adsorption data of erythrosine dye using principal component analysis. Chem Eng J. 2012;191:185-94. DOI: 10.1016/j.cej.2012.03.002.
[30] Ciaburro G. MATLAB for Machine Learning. Packt Publishing Ltd; 2017;374. ISBN: 9781835087695.
[31] Sivanandam SN, Deepa SN. Genetic Algorithm Implementation Using Matlab. In: Sivanandam SN, Deepa SN, editors. Introduction to Genetic Algorithms. Berlin, Heidelberg: Springer; 2008;211-62. DOI: 10.1007/978-3-540-73190-0_8.
[32] Genetic Algorithm Options - MATLAB & Simulink. Available from: https://www.mathworks.com/help/gads/genetic-algorithm-options.html.
[33] Kakhki RM, Mohammadpoor M, Faridi R, Bahadori M. The development of an artificial neural network - genetic algorithm model (ANN-GA) for the adsorption and photocatalysis of methylene blue on a novel sulfur-nitrogen co-doped Fe_2O_3 nanostructure surface. RSC Adv. 2020;10(10):5951-60. DOI: 10.1039/C9RA10349J.
[34] Long R, Xia X, Zhao Y, Li S, Liu Z, Liu W. Screening metal-organic frameworks for adsorption-driven osmotic heat engines via grand canonical Monte Carlo simulations and machine learning. iScience. 2021;24(1):101914. DOI: 10.1016/j.isci.2020.101914.
[35] Etxegarai M, Camps M, Echeverria L, Ribalta M, Bonada F, Domingo X, et al. Virtual Sensors for Smart Data Generation and Processing in AI-Driven Industrial Applications. In: Industry 40 - Perspectives and Applications. IntechOpen; 2022. DOI: 10.5772/intechopen.106988.
[36] Zhao S, Guo J, Tang Y, Zhou Y. Applications of machine learning in heavy metal adsorption modeling: A review. Sep Purif Technol. 2025;377:134168. DOI: 10.1016/j.seppur.2025.134168.
[37] Fan M, Li T, Hu J, Cao R, Wei X, Shi X, et al. Artificial neural network modeling and genetic algorithm optimization for cadmium removal from aqueous solutions by reduced graphene oxide-supported nanoscale zero-valent iron (nZVI/rGO) composites. Materials. 2017;10(5):544. DOI: 10.3390/ma10050544.
[38] Halder G, Dhawane S, Barai PK, Das A. Optimizing chromium(VI) adsorption onto superheated steam activated granular carbon through response surface methodology and artificial neural network. Environ Prog Sustain Energy. 2015;34(3):638-47. DOI: 10.1002/ep.12028.
[39] Mandal S, Mahapatra SS, Sahu MK, Patel RK. Artificial neural network modelling of As(III) removal from water by novel hybrid material. Process Saf Environ Prot. 2015;93:249-64. DOI: 10.1016/j.psep.2014.02.016.
[40] Macena M, Pereira H, Cruz-Lopes L, Grosche L, Esteves B. Competitive adsorption of metal ions by lignocellulosic materials: A review of applications, mechanisms and influencing factors. Separations. 2025:16;12(3):70. DOI: 10.3390/separations12030070.
[41] Huang Z, Liu K, Duan J, Wang Q. A review of waste-containing building materials: Characterization of the heavy metal. Constr Build Mater. 2021;309:125107. DOI: 10.1016/j.conbuildmat.2021.125107.
[42] González-Fernández RA, Leite da Silva AM, Resende LC, Schilling MT. Composite systems reliability evaluation based on Monte Carlo simulation and cross-entropy methods. IEEE Trans Power Syst. 2013;28(4):4598-606. DOI: 10.1109/TPWRS.2013.2267154.

[43] Lin W, Jing L, Zhu Z, Cai Q, Zhang B. Removal of heavy metals from mining wastewater by micellar-enhanced ultrafiltration (MEUF): Experimental investigation and Monte Carlo-based artificial neural network modeling. Water Air Soil Pollut. 2017;228(6):206. DOI: 10.1007/s11270-017-3386-5.
[44] Pathania S, Daksa S, Srinivasan S, Savarimuthu SJX. Automation of adsorption processes using AI: Recent trends and prospects. In: Artificial Intelligence for Multimedia Information Processing. CRC Press; 2024. DOI: 10.1201/9781003405436-16.
[45] Wilson D, del Valle M, Alegret S, Valderrama C, Florido A. Simultaneous and automated monitoring of the multimetal biosorption processes by potentiometric sensor array and artificial neural network. Talanta. 2013;114:17-24. DOI: 10.1016/j.talanta.2013.03.066.
[46] Major Š, Hubálovská M. Virtual laboratories in the teaching of mechanical technology. Chem Didact Ecol Metrol. 2023;28(1-2):135-55. DOI: 10.2478/cdem-2023-0008.